Locating and quantifying the seismic discontinuities in a complex medium through the migration and AVA analysis of reflected and converted waves : an application to the Mt Vesuvius volcano

E. Auger, J. Virieux, A. Zollo

▶ **To cite this version:**

E. Auger, J. Virieux, A. Zollo. Locating and quantifying the seismic discontinuities in a complex medium through the migration and AVA analysis of reflected and converted waves : an application to the Mt Vesuvius volcano. Geophysical Journal International, 2003, 152 (2), pp.486-496. 10.1046/j.1365-246X.2003.01864.x . hal-00406978

HAL Id: hal-00406978
https://hal.science/hal-00406978

Submitted on 29 Jan 2021

HAL is a multi-disciplinary open access archive for the deposit and dissemination of scientific research documents, whether they are published or not. The documents may come from teaching and research institutions in France or abroad, or from public or private research centers.

L'archive ouverte pluridisciplinaire **HAL**, est destinée au dépôt et à la diffusion de documents scientifiques de niveau recherche, publiés ou non, émanant des établissements d'enseignement et de recherche français ou étrangers, des laboratoires publics ou privés.

Geophys. J. Int. (2003) **152,** 486–496

Locating and quantifying the seismic discontinuities in a complex medium through the migration and AVA analysis of reflected and converted waves: an application to the Mt Vesuvius volcano

E. Auger,[1,2] J. Virieux[2] and A. Zollo[1]

[1] *Dip. di Scienze Fisiche, complesso Universitario di Monte S. Angelo,* 80124 *Naples, Italy*
[2] *Géosciences Azur,* 250, *Rue Albert Einstein,* 06560 *Valbonne, France*

Accepted 2002 August 29. Received 2002 July 22; in original form 2001 March 12

Downloaded from https://academic.oup.com/gji/article/152/2/486/654077 by guest on 29 January 2021

SUMMARY

In this paper, we show how the migration of active seismic data can be used to identify and position a seismic discontinuity in a complex medium, and how the amplitude variations of the converted *P* to *S* waves can be interpreted to constrain the seismic velocities below the interface. For the application we turn our attention on Mt Vesuvius, an active volcano threatening a densely populated area. To better define its plumbing system, we investigate a mid-crust seismic discontinuity first identified by Zollo *et al.* (1996, *Science,* **274,** 592–594) and assumed to be the top of a layer containing low-velocity material. We deduce a reference velocity model from previous works on first arrival times, and use it to migrate *PP* reflected and *PS* converted waves. In the migration image, the interface extends at least 20 000 m NE and 20 000 m SW of the volcano, at the depth of 8000 m, and with a mean dip less than 3 per cent. The migration of finite-difference synthetics exclude the fact that the migrated phases interpreted as 8000 m deep reflections or conversions might be multiples in the shallow layers.

The *PS* and first arrival amplitudes are compared at a fixed station and for all the shots to determine the variations of the *P*-to-*S* conversion coefficient with the angle of incidence. It appears to vary very slowly over the whole range of incidence angle at disposal (50°–80°). This implies a dramatic drop of *S*-wave velocity from approximately 3600 m s^{-1} above to less than 1000 m s^{-1} below the interface. The smoothness of the variations indicate that the *P*-wave velocity also diminishes across the interface.

The very low *S*-wave velocity, other geophysical observations at Vesuvius and in other volcanic systems, lead to the conclusion that below the 8000 m discontinuity there is a very extended layer of hot, partially molten material.

Key words: crustal structure, explosion seismology, low-velocity layer, *S* waves, seismic tomography, volcanic structure.

1 INTRODUCTION

Strong reflections from a mid-crust discontinuity have been identified by Zollo *et al.* (1996) under the Mt Vesuvius volcano in Italy, during an active onland seismic survey in 1994. They found a so-called large-amplitude late-arrival (LALA) phase, identified as the *S* conversion of a *P* wave impinging on an almost flat horizontal interface lying at a depth of approximately 10 000 m. A partial deduction from such an observation was the existence of a rather high contrast of shear wave velocity at that depth, interpreted as evidence of partially molten material, maybe magma. Since a good understanding of the Mt Vesuvius magma feeding system is needed to design any realistic eruption scenario, here we investigate the properties of the mid-crustal interface giving rise to the LALA phases. To attain this specific goal we address practical problems that might have a more general relevance: for example, the assessment of the migration image robustness, the interpretation of the wave amplitude variations in terms of velocity contrasts, and the use of the peculiar behaviour of *P*-to-*S* converted waves at wide angle to obtain an accurate image even with an imperfect background velocity model. This paper is more focused on the technical issues, while the volcanological implications of the results have been investigated in a previous publication (Auger *et al.* 2001).

We base our analysis on the data gathered during a mixed offshore/onland experiment performed in 1997 in the Bay of Naples. During this experiment, the Nadir ship run by the French oceanographic institute IFREMER, fired some 1500 air-gun shots every 150 m over an area roughly equal to 5000 km^2, while the registrations were performed onland by 3C temporary stations (Fig. 1).

© 2003 RAS

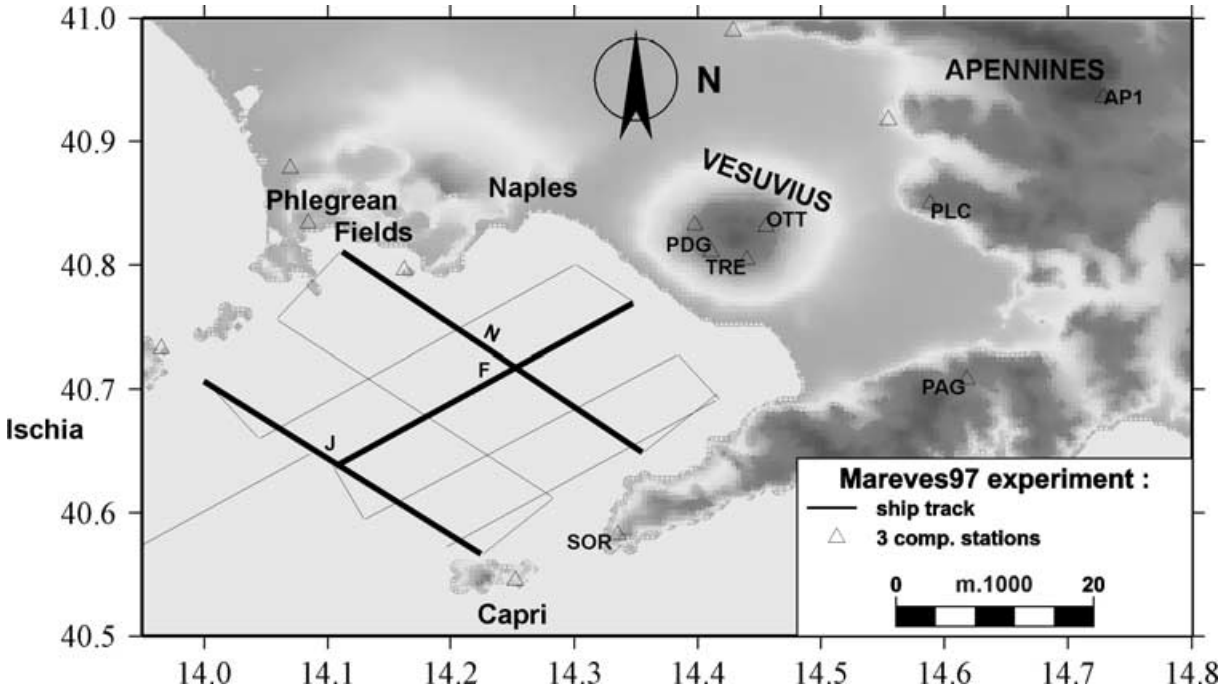

Figure 1. Map of the Vesuvius area with experiment lay-out. The shot profiles used in data preliminary analysis are shown in bold.

Through a preliminary data analysis we first ascertain the presence of mid-crustal reflections and conversions over most of our data set. Then, we restrain the subsequent study to the records of stations PDG, OTT, TRE, PLC and AP1 for the shots of profile *F*, since they densely sample a NE–SW profile passing through the volcano, the shallow structure of which is now better understood thanks to the work performed by the TomoVes group (Gasparini & Group 1998). Based on their results, we draw a careful reference velocity model in which the application of kinematic migration discloses the 2-D in-depth geometry of the LALA interface.

The final part of the paper is devoted to quantifying the seismic velocities below the interface, which is of prime importance for the volcanological interpretation. In a first step we relate the observed amplitude of the *PS* phase to the *P*-to-*S* reflection coefficient at the interface. Then the variations of this coefficient are used to constrain the seismic velocities in the underlying medium.

2 DATA OVERVIEW: FIRST HINTS OF A MID-CRUSTAL 'LALA' REFLECTOR

The data acquisition system has many shots and few stations so that our natural representation is that of common receiver gather (CRG). In order to detect mid-crustal 'LALA' reflections or conversion, we apply an *ad hoc* normal move-out (NMO) correction: it consists in assuming a horizontal interface buried at a given depth in a constant-velocity medium. The propagation time for the reflected or converted phase is then computed via ray tracing. Then each trace in the seismic panel is shifted along the time axis by a time corresponding to the theoretical phase propagation time, minus the propagation time at zero offset. As a result, if the seismic velocities and interface depth are exact, the phase should align at a constant time.†

†Let us note that this correction is different from the classic NMO correction since it does not assume that the propagation time should be proportional to the offset.

We set the *P*-wave velocity at 6000 m s^{-1}, in accordance with the apparent slopes of the phases observed at the furthermost stations. The *S*-wave velocity is given by a constant *Vp*/*Vs* ratio of 1.8, a value that turned out to be optimal for the relocalization of local earthquakes (Bernard, pers. comm, 2001). Following the work of Zollo *et al.* (1996) we first search for an interface at 10 000 m depth. Fig. 2 shows the two CRG gathers AP1 and PLC once the NMO correction has been applied. A coherent phase with significant amplitude can be seen on PLC around the expected reduced time with lateral time undulations. We found the same phase on the AP1 gather, albeit with less intensity, around the same reduced time, which is a clue that the interface is almost horizontal. Note that the time *fluctuations*, identical at both stations, are an evidence of strong lateral velocity inhomogeneity in the vicinity of the shots that will have to be included in the reference velocity model.

This simple analysis argues for the presence of *P*-to-*S* conversions occurring at roughly 10 000 m depth. We now apply the same type of NMO correction to look for *P*-to-*P* reflections (Fig. 3). The gathers of SOR for profile *J* and *N* and PAG and AP1 for profile *F* all exhibit a prominent arrival around the predicted time (3.3 s), better seen at greater offsets, which is consistent with a *PP* phase undergoing subcritical reflection at wide angle. We could not identify unambiguously *PS* or *PP* phases for the stations lying on Vesuvius and in the Phlegrean Fields, probably because the strong superficial velocity heterogeneity in these areas contradicts the hypothesis of homogeneous propagation underlying the NMO correction.

3 DATA MIGRATION: DRAWING UP A 2-D IN-DEPTH IMAGE OF THE LALA REFLECTOR

We will obtain an image of the interface through the application of a depth migration technique known as the RAY+BORN

Downloaded from https://academic.oup.com/gji/article/152/2/486/654077 by guest on 29 January 2021

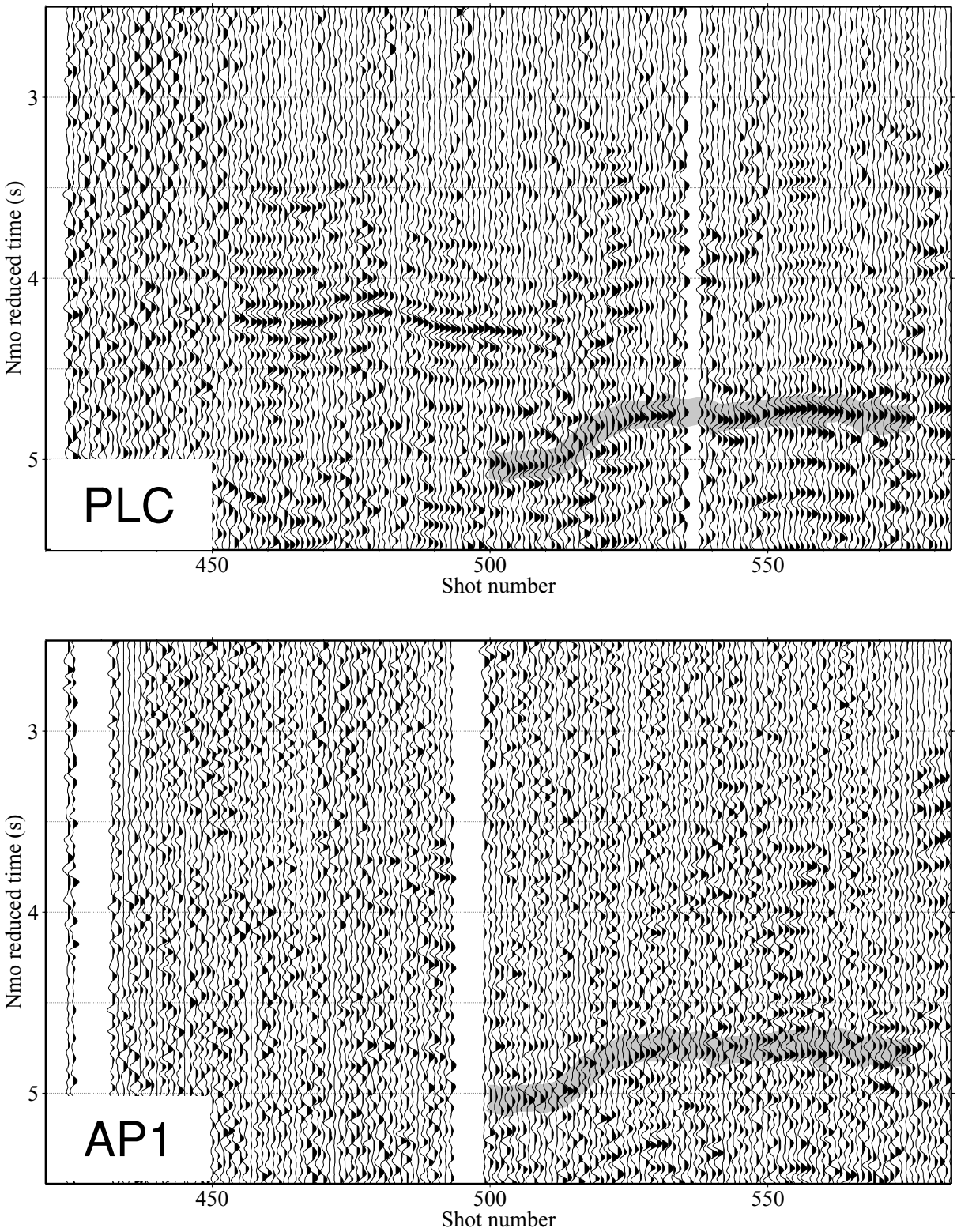

Figure 2. Horizontal ground velocity observed at the stations PLC and AP1 for the shots of profile *F*. The ray-NMO correction applied should align *PS* phases at 4.66 s, and the identified energetic phases are underlined in grey.

method, which has been shown to focus reflected energy below heterogeneous velocity structures (Thierry *et al.* 1999). It requires a background velocity model to compute traveltimes via ray tracing.

3.1 Preferred reference velocity model

When building our preferred reference velocity model (Fig. 4), we take advantage of the recent seismic tomography studies carried out

Downloaded from https://academic.oup.com/gji/article/152/2/486/654077 by guest on 29 January 2021

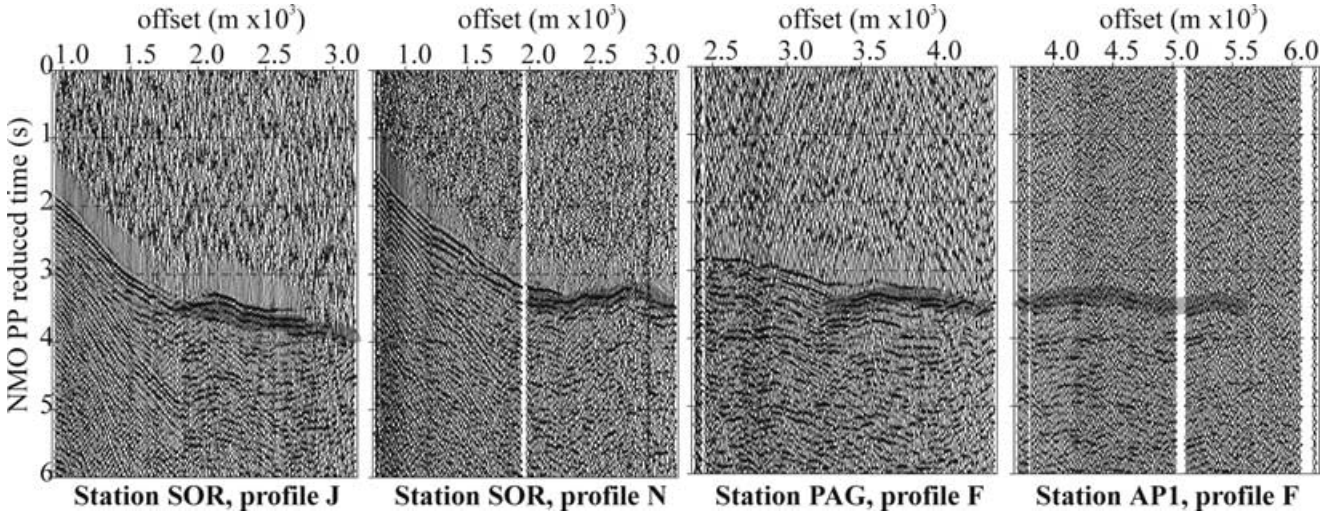

Figure 3. Ray-NMO correction for *PP* phases applied at various CRG with a 3-D distribution. Note the systematic presence of a prominent phase around the theoretical alignment time (3.3 s), with amplitude increasing at larger offsets.

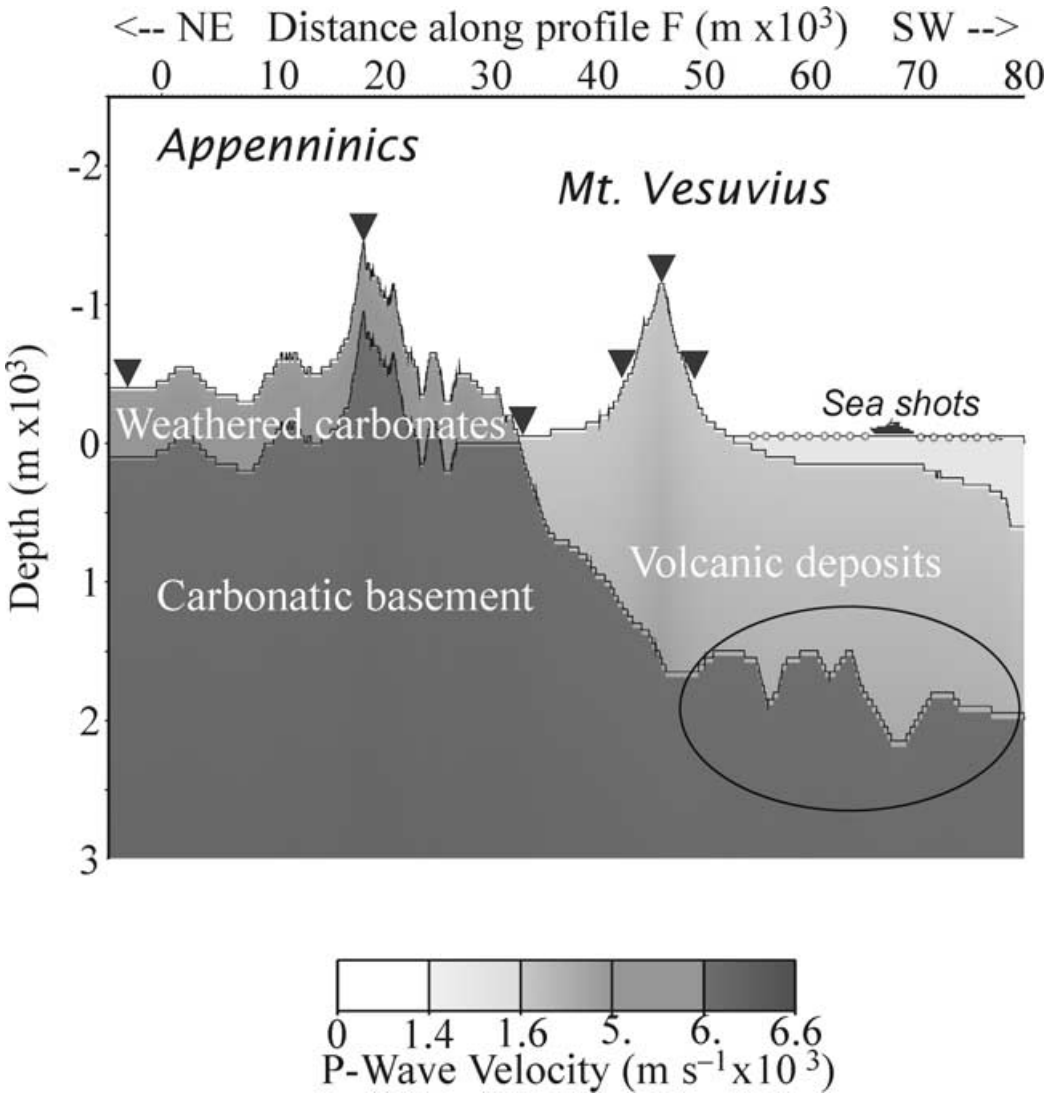

Figure 4. Preferred velocity model (see Table 1) used for 2-D migration. The shape of the interface between volcanic deposits and the carbonatic basement inside the ellipse is fine-tuned by matching the first arrival times at two stations lying on Vesuvius. Black triangles denote the stations used to obtain the migrated image. Vertical exaggeration × 4.

Downloaded from https://academic.oup.com/gji/article/152/2/486/654077 by guest on 29 January 2021

Table 1. Preferred velocity model.

Type of lithology	Velocity at top of layer (m s^{-1} × 10^3)	Vertical velocity gradient (s^{-1})
Sea water	1.5	0.0
Volcanic deposits	1.7 (+8 per cent at sea)	0.7 (+8 per cent at sea)
Weathered outcropping	4.5	3.0
carbonates	4.5	3.0
Carbonatic basement	6.0	0.05

by the TomoVes working group (Gasparini & Group 1998). Our model is basically made up of two bodies, representing the volcanic deposits and the carbonatic sediments, respectively. In each layer the velocity is given by the velocity at the top of the layer, and the vertical velocity gradient (Table 1). The *S*-wave velocities, as before, are described by a constant Vp/Vs ratio of 1.8.

For the volcanic deposits in the central zone of the volcano, the velocity parameters are chosen in accordance with the τ–p analysis of first arrival times (De Matteis *et al.* 2000). At sea, where no information is available, the same velocities are assumed, with an 8 per cent increase. This value, determined through trial and error, gives the best focused migration image.

In the carbonatic basement, we choose the initial velocity as the apparent velocity on the records of the furthermost AP1 station. We also apply a low vertical gradient (0.05 s^{-1}) as the mean value for the uppermost crust in this area. In the weathered carbonates outcropping at the NE end of the profile, a low velocity and a strong gradient are assigned to a very thin layer of superficial material, chosen in accordance with the results of 2-D seismic tomography in this area (Herrero *et al.* 1999; Zollo *et al.* 2000).

A strong velocity contrast exists at the interface between the carbonates and the volcanic deposits. Therefore, the accurate traveltime prediction requires the faithful description of the shape of this interface. Under the Vesuvius volcano, it is provided by the Preliminary Reference Vesuvius Model constrained by low-angle reflection seismics and gravimetric measurements. At sea, it is modified through trial and error until the synthetic arrival times of the refracted wave along that interface match the observed first arrival times on stations OTT and TRE for the shots of profile *F* (Latorre, pers. comm, 2000). The irregular shape of this interface we determine in this way accounts for the high-frequency time fluctuations of the phases identified in the preliminary data analysis.

3.2 A 2-D in-depth image of the interface from *PP* and *PS* migration

In this background velocity model, we apply the RAY+BORN migration technique to the data consisting of the shot profile *F* and five onland stations. For *PS* (respectively, *PP*) migration the longitudinal (respectively, vertical) component of the records is used. Each type of migration applied to a single station illuminates a different portion of the interface, and the global migration image (Fig. 5) is obtained by summing the partial contributions.

The final image exhibits a clear, global and elongated increase of energy at the depth of roughly 8000 m, all the way from Vesuvius to the Apenines. The sum of image intensity along horizontal lines presents a sharp peak in correspondence with the detected energy increase—a demonstration of the satisfying degree of focusing that we have attained. The remaining scattering of some migrated phases can be associated with 3-D effects, the PLC station lying off the profile, or to second-order imperfections of the velocity model. To obtain this image we applied a slope window of between 80° and 110° with respect to the vertical, as suggested by the data preliminary analysis that identified an almost flat reflector. In fact, any true slope would prevent the nearly horizontal alignment that is

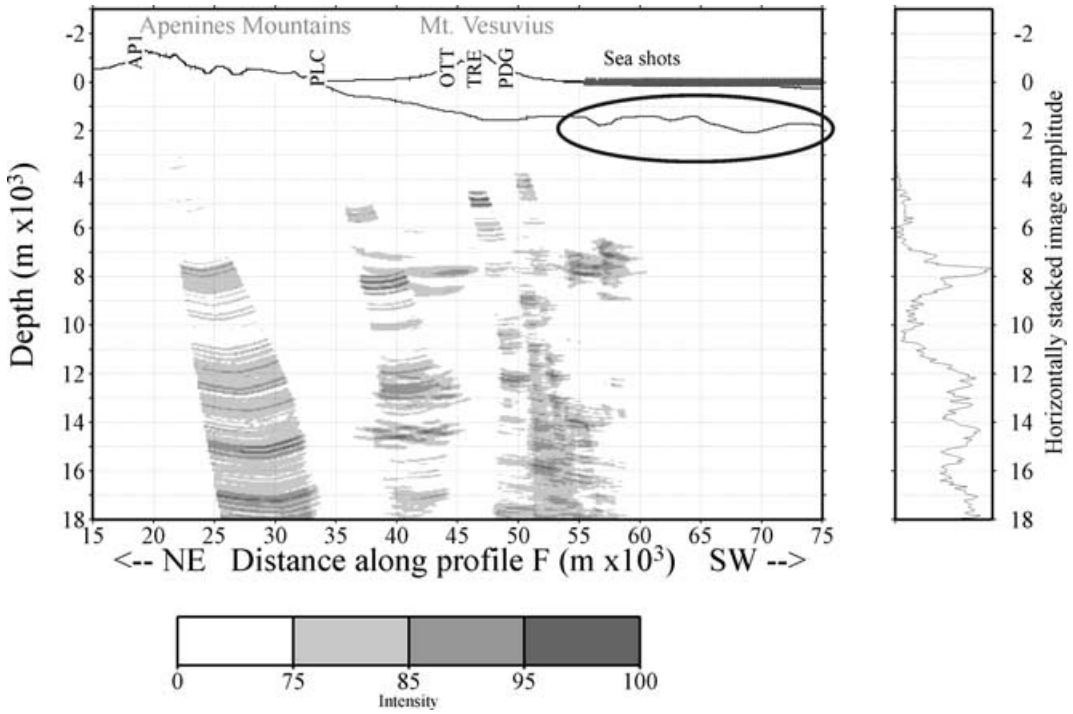

Figure 5. Migration of *PP* and *PS* phases at stations AP1, PLC, OTT, TRE and PDG for the shots of profile *F*. (left). The sharp peak in the horizontal image summation (right) indicates the good focusing of the waves reflected and converted at 7900 m depth. The ellipse encloses the part of the interface retrieved through *PS* migration at station AP1 This figure was adapted from fig. 3 of Auger *et al.* (2001).

Downloaded from https://academic.oup.com/gji/article/152/2/486/654077 by guest on 29 January 2021

observed at 8000 m on the migration image, a justification of the dip-windowing. We are rather confident that the detected increase of energy delineates a real discontinuity and is not a migration artefact, since it is made up of images of *PS* and *PP* phases that were recorded at stations as much as 30 000 m apart, and located on both sides of the volcano and on the first carbonatic outcrop. With respect to the preliminary data analysis, we now find the interface at a lesser depth (8000 m instead of 10 000 m). The reason for this is that we now use a slower velocity model that includes the slow layers of volcanic deposits and marine sediments. Finally, looking at the migrated image of the *PS* phase detected in AP1 (Fig. 5), we observe how the migrated *PS* phases collapse in a narrow zone of the interface almost upright to the receiver. It follows that the minimal extension of the interface 35 000 m is well constrained by the position of the stations at which *PS* phases are observed.

At shallower depths, the backpropagated energy does not exhibit any consistent geometrical pattern, and should therefore be attributed to misinterpreted phases, such as a first arrival migrated as *PP* or *PS*. Below the interface, energetic signals appear but cannot be interpreted, since the current velocity model does not include any velocity change below the interface we have retrieved. We may speculate that these later arrivals come either from another deeper interface, or from shallow multiples created by superficial reflections between the free surface and the 8000 m LALA discontinuity.

3.3 Synthetic test of the origin of the LALA phases

The volcanic structure presents a strong superficial complexity, so that the phases we identified as reflections at the 8000 m LALA interface might, in fact, be multiple reflections in the volcanic layer. This hypothesis has already been ruled out by Zollo *et al.* (1996), using simple synthetic finite-difference propagation simulations. We go one step further and apply our migration technique to full wavefield finite-difference synthetic seismograms computed in the more complete velocity model now available without the LALA interface. Then, we migrate these synthetic data back into the medium (Fig. 6). The shallow energy focusing results from the interpretation as *PP* or *PS* phases of first arrivals, and there is no focusing of energy around 8000 m. This suggests that the LALA energy in Fig. 5 is not related to any feature of the background velocity model, in particular the interface between carbonate and volcanic deposits. This simple synthetic test argues very strongly in favour of the existence of the LALA reflector.

4 THE QUEST FOR THE SEISMIC VELOCITIES BELOW THE LALA INTERFACE

We are now going to put some constraints on the velocities below the LALA interface through the study of *PS* amplitudes. We will take the following steps: first, relate the observed *PS* amplitude variations at a fixed station to the variations of the *P*-to-*S* conversion coefficient when the incidence angle changes at the interface. Secondly, select the *P* and *S* velocities in the lower medium associated with a theoretical conversion coefficient compatible with that retrieved at the first step.

4.1 Experimental *PS* conversion coefficient variation

Many effects contribute to the observed amplitude of the *PS* phase amplitude: the *P*-to-*S* conversion coefficient that we want to isolate, but also the propagation in the vicinity of the sources and the receiver, the transmission through the carbonatic/volcanic interface, and the wave geometrical divergence undergone in the carbonatic basement. Most of these effects would be very difficult to model, and the solution we propose is to study jointly the observed amplitude of the first arrival, hereafter referred to as the *FA* phase. The reason for this is that most of the propagation effects are common to the two types of phase, or identical for all shots. This can be seen by considering the rays traced in Fig. 7, and we show in the appendix that, consequently, the *P*-to-*S* conversion coefficient for the shot i, R_i, can be written in the following way:

$$R_i = a \frac{A_i^{PS}}{a_i^{FA}} \frac{D_i^{FA}}{D_i^{PS}}. \quad (1)$$

In this expression D_i^{PS} and D_i^{FA} represent the geometrical divergences undergone in the carbonates only, and can be computed. A_i^{PS} and A_i^{FA} denote the observed phase amplitudes at a fixed station, and

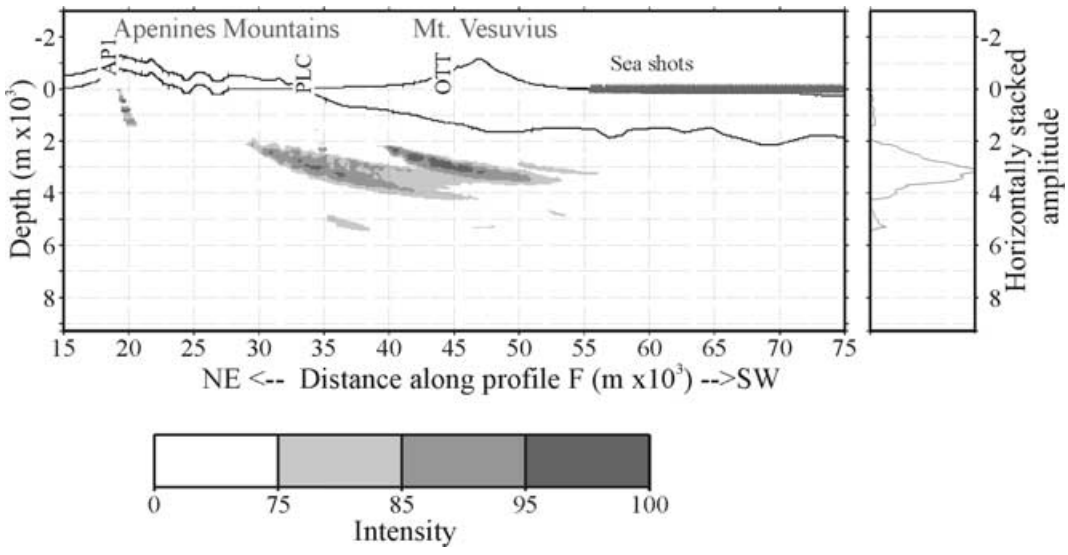

Figure 6. Migration of full-wavefield elastic finite-difference synthetics computed in the preferred velocity model, without a LALA interface. No energy is backpropagated where the LALA interface is seen on the data image (Fig. 5).

Downloaded from https://academic.oup.com/gji/article/152/2/486/654077 by guest on 29 January 2021

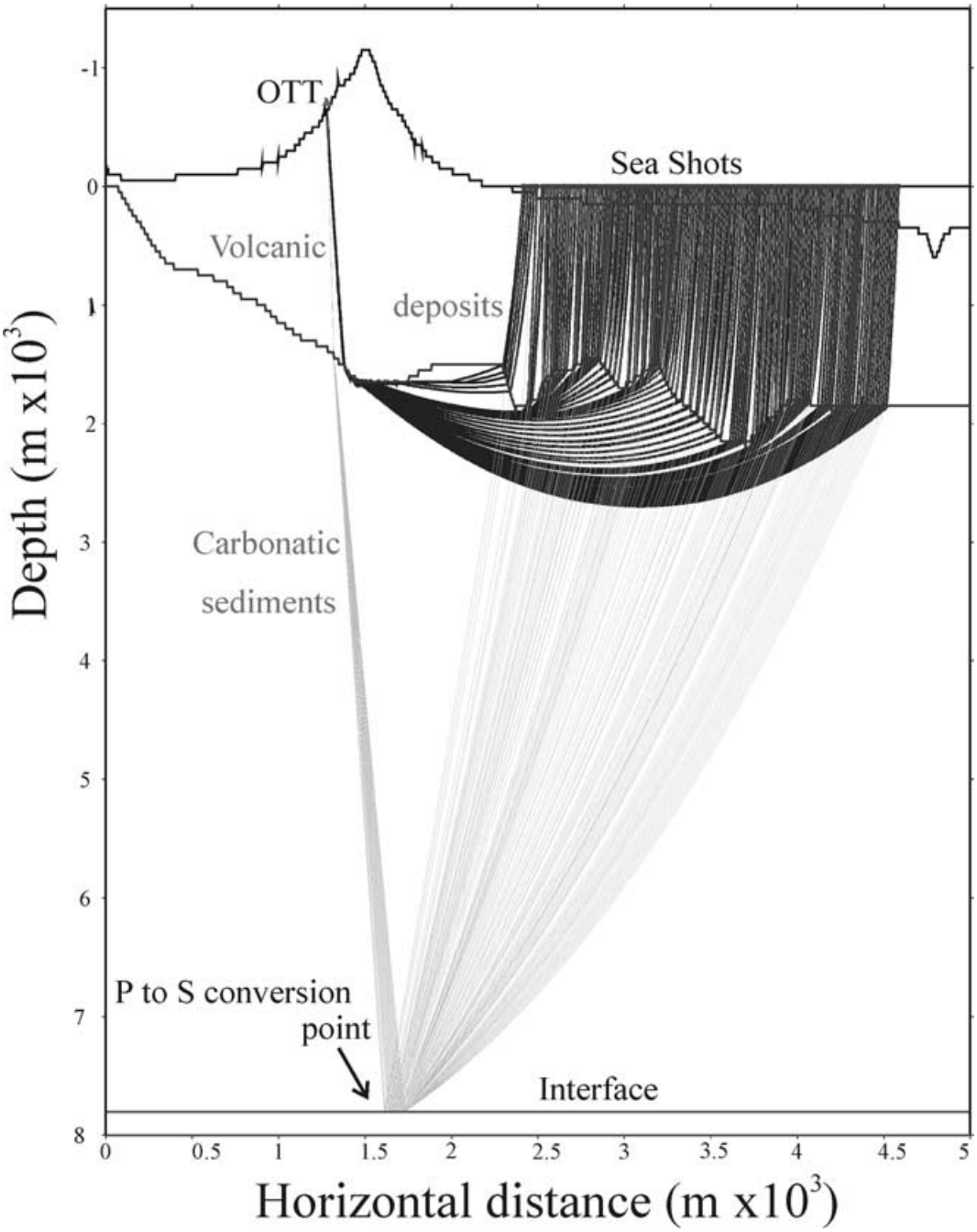

Figure 7. Rays of the *PS* phase and the first arrival at OTT. Note that the paths of the two phases are almost the identical in the marine sediments.

a is a factor containing all the propagation effects that do not depend on the shot number. We can now normalize eq. (1) to its sum over all the shots to remove *a*, and obtain the experimental *variations* of the conversion coefficient through the computation of the geometrical divergences and the measurement of the phase amplitudes.

Raw measurements of *FA* and *PS* amplitude at the OTT station are shown in Fig. 8. To each source we have associated the corresponding incidence angle at the reflector, taking into account the interface model obtained through migration (Fig. 5). Raw curves present an important scattering with respect to the incident angle on to the LALA interface, but a nice correlation between the two curves can be seen. As far as the high-frequency content is concerned, a sharp peak in the amplitude of one of the two phases is immediately followed or preceded by a peak in the other phase. This correlated behaviour is the effect of the common propagation in the marine sediments near the shots (Fig. 7).

We apply a moving average smoothing technique to the two raw curves and find a common monotonic decrease, consistent with the increasing distance from shots. The amplitude ratio (short dotted curve in Fig. 8) is found to be almost constant throughout the 30° wide angular interval investigated. Finally, we plot the measured *PS* amplitude versus the measured *FA* amplitude after normalization in Fig. 9, and observe a strikingly linear trend. This trend confirms the constant value found previously for the amplitude ratio, and seems to be very consistent for the two stations. Consequently, the measured amplitude ratios can be considered to be

Downloaded from https://academic.oup.com/gji/article/152/2/486/654077 by guest on 29 January 2021

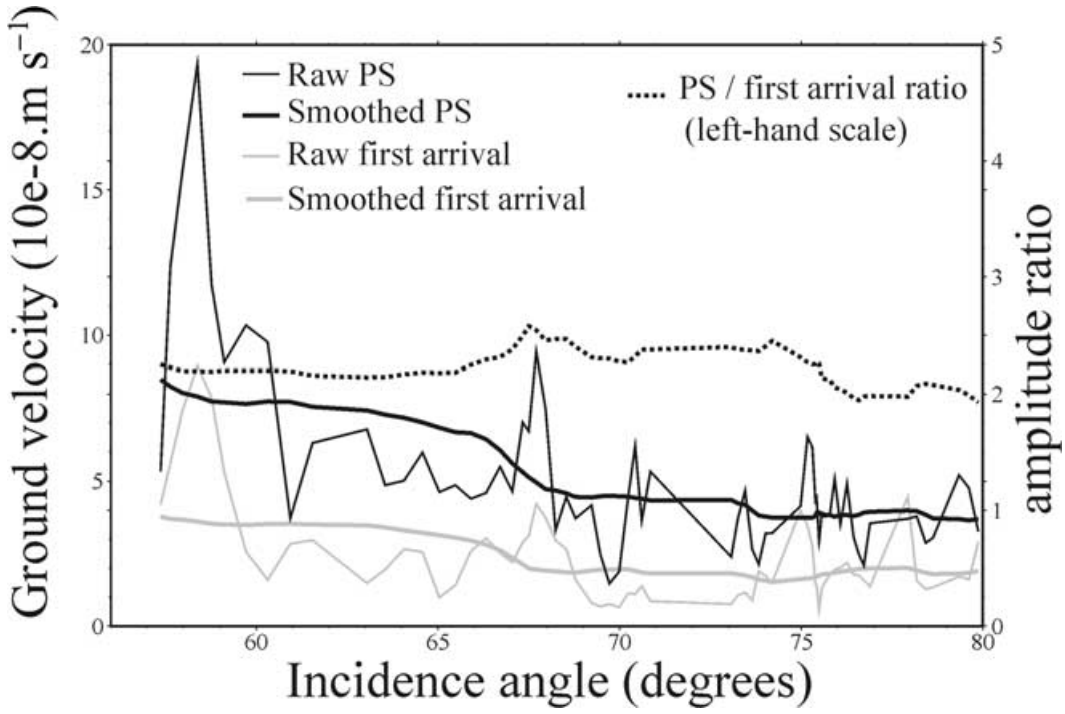

Figure 8. Raw and smoothed amplitudes of the *PS* and first arrival at station OTT as a function of the incidence angle at the interface. Note that the ratio of the smoothed amplitudes (left-hand scale) keeps an almost constant value over the 30° angle range.

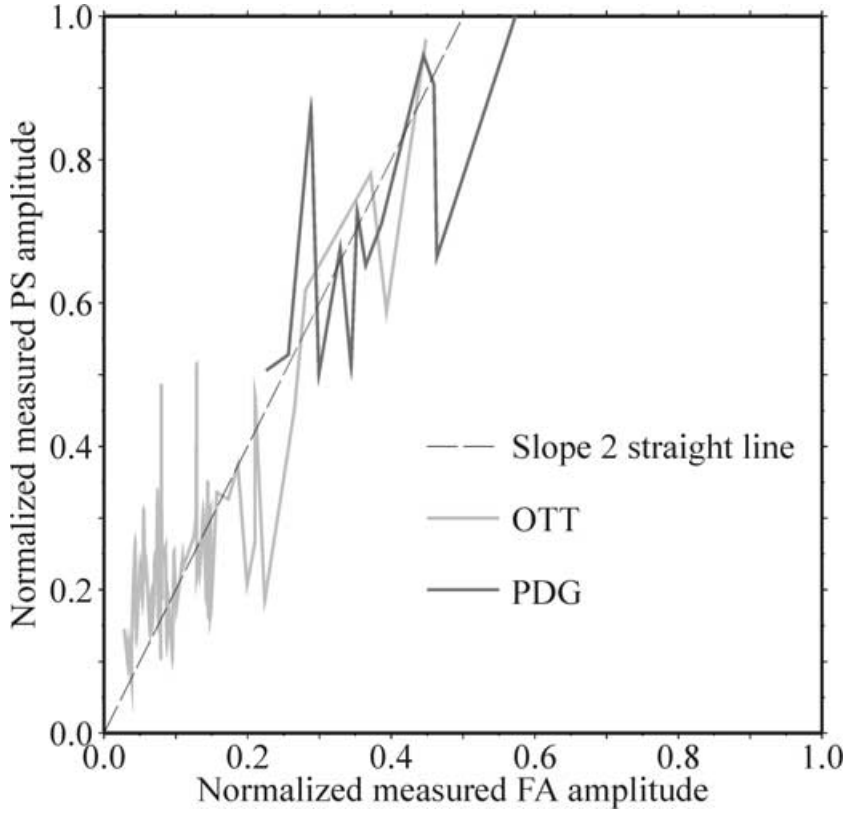

Figure 9. Raw *PS* amplitudes plotted versus the raw *FA* amplitudes for stations OTT and PDG. The clear linear trend is a sign of the measurements consistency, and confirms the constant value for the ratio *PS/FA*. This ratio seems to be the same for both stations, arguing for the lateral homogeneity of the medium underlying the LALA interface.

Downloaded from https://academic.oup.com/gji/article/152/2/486/654077 by guest on 29 January 2021

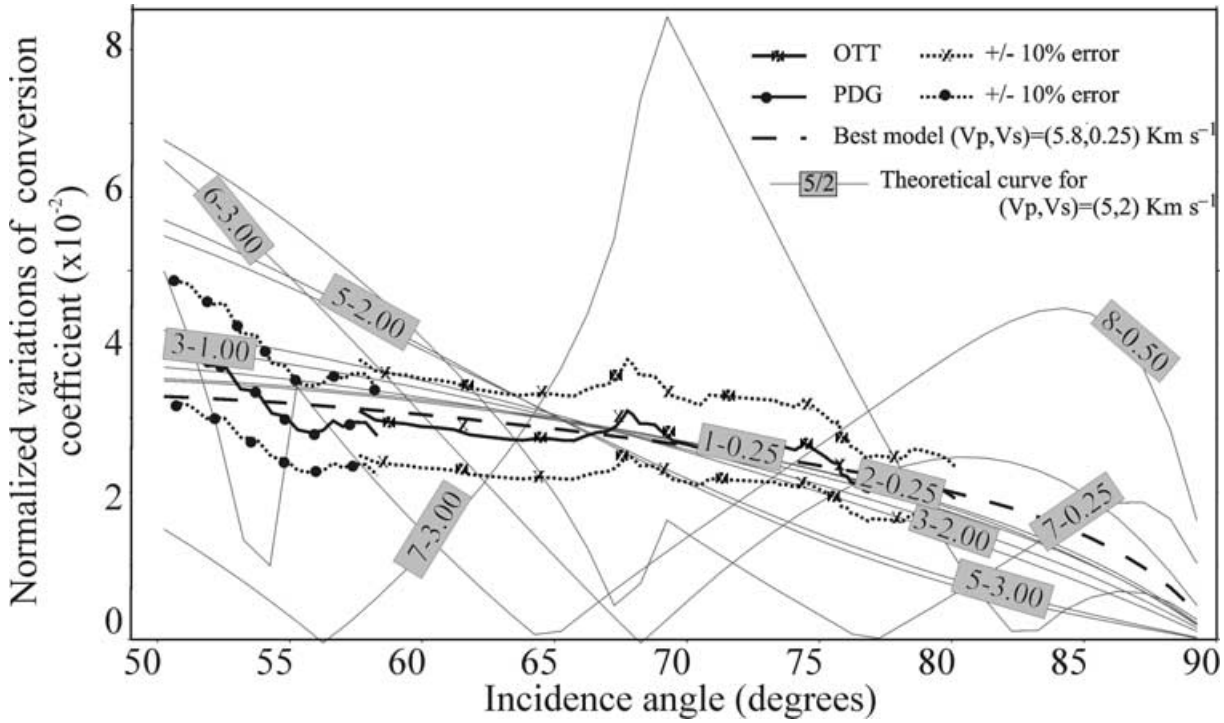

Figure 10. Abacus of *P*-to-*S* conversion coefficient normalized variations associated to various *P* and *S* velocities in the underlying medium. Also represented the experimental curves associated to stations OPT and PDG, with their ±10 per cent relative error interval. The almost constant *PS/FA* ratio implies very slowly varying experimental curves, which in turn means that the *S* velocity is very low below the LALA interface.

independent of the selected station, and we shall mix them together in the following investigation of the velocities below the LALA interface.

4.2 Interpretation of the experimental conversion coefficient

We will constrain the velocities in the underlying medium by assuming different values, and comparing the associated theoretical conversion coefficient variations (Aki & Richards 1980) with the experimental curve retrieved in the previous section.

At the interface depth, in our velocity model, the *P*-wave velocity is 6500 m s^{-1} and the *S*-wave velocity is 3610 m s^{-1} in the carbonates immediately above.‡ Fig. 10 displays both different theoretical curves and the experimental data relative to the OTT and PDG stations. Let us remark that, whenever the *P* velocity is assumed to be higher in the underlying medium, we observe jumps in the theoretical curves as a result of critical conversion. In contrast, the experimental curve is always smooth. The sharp variations in raw *FA* and *PS* measurements of Fig. 8 have been explained as a source effect rather than a critical conversion, because they were observed on both *FA* and *PS* amplitudes. From this rather smooth

‡In the following we assume an equal density below and above the interface, corresponding to the physical hypothesis that the underlying medium is made of partially molten magma in lithostatic equilibrium. In contrast, assuming for the underlying medium the density of flyschoid sediments found at that depth in the nearby Apenninic chain leads to a null *S*-wave velocity contrast across the interface, which is unable to create the strong *P*-to-*S* conversions observed.

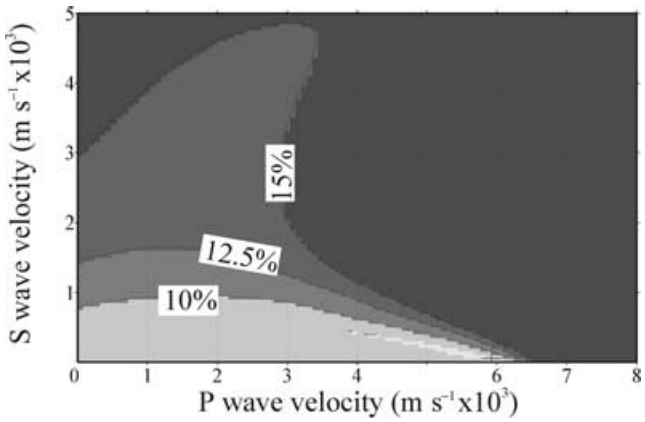

Figure 11. Relative misfit between experimental and theoretical normalized variations of the *P*-to-*S* conversion coefficient as a function of the *P* and *S* velocity assumed in the medium underlying the LALA interface. Only very low *S* velocities, less than 1000 m s^{-1}, are associated with a relative error of less than 10 per cent.

behaviour of the conversion coefficient, we expect the *P*-wave velocity to decrease through the interface. Let us also note the *very slow diminution* of the conversion coefficient along the angular range: it constrains the *s*-wave velocity to be very low below the interface.

We perform a systematic grid search of the best-fitting *P*- and *S*-wave velocities, and in Fig. 11 we plot the error with respect to data for all the models. In this diagram, the 10 per cent relative error isovalue encloses all the velocity models with a probability higher than 90 per cent. With this error threshold, the *S*-wave velocity is constrained to very low values, less than 1000 m s^{-1}. In contrast the *P* velocity is wildly unresolved, and the only

Downloaded from https://academic.oup.com/gji/article/152/2/486/654077 by guest on 29 January 2021

information we may trust concerning it is that it decreases across the interface.

5 RESULT SUMMARY AND IMPLICATIONS CONCERNING THE MAGMA FEEDING SYSTEM OF VESUVIUS

In summary, a rough preliminary analysis of the data from an active seismic experiment carried out in the Bay of Naples, gives strong evidence of *PP* reflected and *PS* converted phases coming from a mid-depth interface under Vesuvius, i.e. the so-called LALA. Based on previous tomography studies in the area, we define an accurate velocity model along a 2-D NE–SW profile passing through the volcano. In this model, kinematic data migration provides an in-depth image of the discontinuity: it appears to be flat, at roughly 8000 m depth, and extends at least 25 000 m NE and 10 000 m SW of the crater of the volcano. No other large seismic discontinuity is detected between that interface and the volcanic sediments. Through the migration of full wavefield synthetics we assess that LALA phases are not misinterpreted multiples in the shallow structure of the volcano.

We also infer from the picked amplitude of the *PS* phase the variations of the *P*-to-*S* conversion coefficient with the angle of incidence. These can constrain the propagation velocities below the interface. It stems that the *P*-wave velocity is less below than above the interface, and that the *S*-wave velocity, which is rather well resolved, should be less than 1000 m s^{-1}.

The presence under volcanic structures of mid-depth seismic discontinuities consisting in a sharp decrease of *S*-wave velocity is an increasingly accepted feature. In fact, since the pioneering work of Sanford on the Socorro volcano, many studies of passive seismic records have led to the conclusion that only such discontinuities can account for the detection of prominent converted *S* phases. The reader may refer to Matsumoto & Hasegawa (1996) for the Nikko-Shirane in Japan, Cruz-Atienza *et al.* (2000) for the Popocatepetl in Mexico, and Stroujkova & Malin (2000) for the Casa Diablo caldera in the USA, while Negishi & Horiuchi (2000) detects a low-*Q* zone in the depth range 5000–9000 m under the Usu volcano in Japan. The lateral extension of the LALA interface is not unusual either, considering that Balch *et al.* (1997) evaluates to 3400 km^2 the area covered by the mid-crustal discontinuity under the Socorro.

As far as Vesuvius is concerned, the reader may refer to Auger *et al.* (2001) for a detailed volcanological interpretation of the LALA reflector. Basically, we think that the very low *S*-wave velocity in the medium underlying the LALA interface is an indication that it contains hot, possibly partially molten, material. It would be consistent with the detection of a 7000 m deep conductive anomaly under the volcano through the analysis of the magnetotelluric field (Di Maio *et al.* 1998), and the local earthquakes cut-off depth—4000 m according to the most recent studies (Lomax *et al.* 2000)—which indicates that brittle mechanical behaviour no longer occurs at the LALA depth.

Petrological evidence further suggest that the LALA body may play an important part in the volcano feeding system: the entrapment pressures of fluid inclusions in erupted minerals are consistent with the 4000–10 000 m depth range, and the isotopic ratios of Ka strongly argue for a twofold origin of the materials erupted during the strongest subplinian events. Therefore, we believe that the LALA body may represent a second, deep and extended magma reservoir feeding Vesuvius.

ACKNOWLEDGMENTS

This work was in part funded by the European Community, Directorate General XII, under contract n° ENV4-CT96-5015, and in part by two grants from the Italian Gruppo Nazionale per la Vulcanologia.

REFERENCES

Aki, K. & Richards, P., 1980. *Quantitative Seismology: Theory and Methods.* Freeman, San Francisco.

Auger, E., Gasparini, P., Zollo, A. & Virieux, J., 2001. Seismic evidence of and extended magamatic sill under Mt Vesuvius, *Science,* **294,** 1510–1512.

Balch, R.S., Hartse, H.E., Sanford, A.R. & Lin, K.-W., 1997. A new map of the geographic extent of the Socorro mid-crustal magma body, *Bull. seism. Soc. Am.,* **87,** 174–182.

Cruz-Atienza, V.M., Pacheco, J.F., Shapiro, N.M., Sing, S.K., Iglesias-Mendoza, A. & Valdes, C., 2000. Size of Popocatepetl volcano explosions from waveforms inversion, in *Expanded Abstracts.* American Geophysical Union.

De Matteis, R., Latorre, D., Zollo, A. & Virieux, J., 2000. 1D/2D *p*-velocity models of Mt Vesuvius volcano from the inversion of TomoVes96 first arrival time data, *Pure appl. Geophys.,* **157,** 1643–1661.

Di Maio, R., Mauriello, P., Patella, D., Petrillo, Z., Piscitelli, S. & Siniscalchi, A., 1998. Electric an electromagnetic outline of the Mt Somma–Vesuvius structural setting, *J. Volc. Geotherm. Res.,* **82,** 219–238.

Gasparini, P. & Group, T.W., 1998. Tomoves: a project of seismic investigation of Mt Vesuvius, *EOS, Trans. Am. geophys. Un.,* **79,** 229–231.

Herrero, A., Zollo A. & Virieux, J., 1999. 2-D non linear first arrival time inversion applied to Mt Vesuvius active seismic data (TomoVes96). European Geophysical Society annual meeting.

Lomax, A., Zollo, A., Capuano, P. & Virieux, J., 2000. A 3D velocity model for earthquake location under the vesuvius volcano. European Geophysical Society annual meeting.

Matsumoto, S. & Hasegawa, A., 1996. Distinct *s* wave reflector in the mid-crust beneath Nikko–Shirane volcano in the northeastern Japan arc, *J. geophys. Res.,* **101,** 3067–3083.

Negishi, H. & Horiuchi, S., 2000. Large v_p/v_s and low-*q* region beneath the Usu volcano area, Hokkaido, Japan, in *Expanded Abstracts.* American Geophysical Union.

Stroujkova, A.F. & Malin, P.E., 2000. A magma mass beneath Casa Diablo? Further evidence from reflected seismic waves, *Bull. seism. Soc. Am.,* **90,** 500–511.

Thierry, P., Operto, S. & Lambaré, G., 1999. Fast 2D ray-born inversion/migration in complex media, *Geophysics,* **64,** 162–181.

Zollo, A. *et al.*, 1996. Seismic evidence for a low velocity zone in the upper crust beneath Mt Vesuvius, *Science,* **274,** 592–594.

Zollo, A., de Matteis, R., Auria, L.D. & Virieux, J., 2000. A 2-D Non Linear Method for Travel Time Tomography: Application to Mt Vesuvius Active Seismic Data, in *Problems in Geophysics for the next millenium*, eds Boschi, E., Ekstroem, G. & Morelli, A., ING-Ed, Compositoi, 2000.

APPENDIX

In this appendix we shall show that complex propagation effects, such as the attenuation in the marine sediments below the shots at sea, need not be modelled to isolate the contribution of the *P*-to-*S* conversion coefficient in the observed amplitude of the *PS* phase. On the contrary, for some simple geometrical arguments based on ray tracing (Fig. 7), we will see that most propagation effects just cancel out when considering the ratio of the amplitudes of the *PS* converted and the first arrival.

Downloaded from https://academic.oup.com/gji/article/152/2/486/654077 by guest on 29 January 2021

More specifically we will write for the observed amplitude of the *PS* phase for the shot i, A_i^{PS}:

$$A_i^{PS} = \mathrm{src}_i^{PS}\,\mathrm{transDown}_i^{PS}\,\mathrm{transUp}_i^{PS}\,\mathrm{sta}_i^{PS}\,R_i^{PS}, \tag{A1}$$

where src_i^{PS} represents the source effect for shot i, including the propagation down to the carbonates, $\mathrm{transDown}_i^{PS}$ the transmission coefficient at the interface between the marine sediments and the carbonates, D_i^{PS} the total geometrical divergence undergone in the carbonates, before and after the conversion at the LALA interface. The term $\mathrm{transUp}_i^{PS}$ is the transmission coefficient at the interface between the carbonates and the volcanic deposits, sta_i^{PS} the attenuation undergone from this interface up to the free surface, including local effects close to the station, and R_i^{PS} is what we try to isolate, the *P*-to-*S* conversion coefficient at the LALA interface.

Similarly, we can model the amplitude of the first arrival (hereafter referred to as *FA* for the same shot i, A_i^{FA}:

$$A_i^{FA} = \mathrm{src}_i^{FA}\,\mathrm{transDown}_i^{FA}\,D_i^{FA}\,\mathrm{transUp}_i^{FA}\,\mathrm{sta}_i^{FA}. \tag{A2}$$

Now, because of the particular geometry of the propagation (*cf.* Fig. 7) we will make the following approximations.

(1) The source terms are the same for both type of wave: $\mathrm{src}_i^{PS} = \mathrm{src}_i^{FA}$. In fact, for each shot, the two phases share a common path in the marine sediments.

(2) The station effects, albeit different for the *PS* and *FA* phases, do not depend on the specific shot, namely $\mathrm{sta}_i\ PS = \mathrm{sta}\ PS$ and $\mathrm{sta}_i^{FA} = \mathrm{sta}^{FA}$. To justify this approximation the ray paths in the volcanic deposits are identical whatever the shot for the two phases. The same approximation can be made for the upward transmission coefficients between the carbonates and the volcanic edifice, since the rays arrive on the interface at almost constant inclination, and leave it along the same path: $\mathrm{transUp}_i^{PS} = \mathrm{transUp}^{PS}$ and $\mathrm{transUp}_i^{FA} = \mathrm{transUp}^{FA}$. We will further assume that the same can be said for the downward transmission coefficient applicable at the interface between the marine sediments and the carbonates: $\mathrm{transDown}_i^{PS} = \mathrm{transDown}^{PS}$ and $\mathrm{transDown}_i^{FA} = \mathrm{transDown}^{FA}$. There is no geometrical justification for this, but we verified the absence of correlation between the observed amplitudes of the phases on the one hand, and the morphology of the interface as retrieved by first arrival time analysis on the other hand.

Taking into account these approximation we obtain an expression of the *P*-to-*S* conversion coefficient by dividing eqs (2) and (3):

$$R_i = \frac{\mathrm{transDown}^{PS}}{\mathrm{transDown}^{FA}}\,\frac{\mathrm{transUp}^{PS}}{\mathrm{transUp}^{FA}}\,\frac{\mathrm{sta}^{PS}}{\mathrm{sta}^{FA}}\,\frac{A_i^{PS}}{A_i^{FA}}\,\frac{D_i^{FA}}{D_i^{PS}}$$

$$= a\,\frac{A_i^{PS}}{A_i^{FA}}\,\frac{D_i^{FA}}{D_i^{PS}},$$

where a does not depend on the shot i. This is eq. (1) from which we retrieve the variations of the conversion coefficient.

Downloaded from https://academic.oup.com/gji/article/152/2/486/654077 by guest on 29 January 2021